J Solid State Electrochem
DOI 10.1007/s10008-015-3047-9

ORIGINAL PAPER

Novel $La_{2-x}Cu_xNiO_{4\pm\delta}/La_4Ni_3O_{10-\delta}$ composite materials for intermediate temperature solid oxide fuel cells, IT-SOFC

Mosbah Ferkhi[1,2] · **Armelle Ringuedé**[2] · **Michel Cassir**[2]

Received: 12 June 2015 / Revised: 22 September 2015 / Accepted: 27 September 2015

Abstract Phases constituted by $La_{2-x}Cu_xNiO_{4\pm\delta}$ ($0.01 \leq x \leq 0.1$) of the Ruddlesden-Popper family ($La_{n+1}Ni_nO_{3n+1}$; $n=1$) were prepared and then mixed with $La_4Ni_3O_{10}$, in a weight ratio of 50:50 wt%, in order to be used as solid oxide fuel cell cathodes. ASR values relative to the symmetrical cells constituted by yttria-stabilized zirconia electrolyte and the following electrodes, $La_{1.98}Cu_{0.02}NiO_{4+\delta}+La_4Ni_3O_{10}$ and $La_{1.95}Cu_{0.05}NiO_{4+\delta}+La_4Ni_3O_{10}$, are of 11.8 Ω cm^2 at 650 °C for both and, respectively, of 3.5 and 2.9 Ω cm^2 at 750 °C. In the case of the second cell, the electrode material reacts with the electrolyte forming an insulating phase at the interface, contrarily to the first cell, which stability could be explained by the combination of low doping amounts of copper and the presence of $La_4Ni_3O_{10}$ acting as a stabilizer of the material at high temperature.

Keywords Composite materials · Ruddlesden-Popper · SOFC · Sol–gel · Impedance spectroscopy

This paper is dedicated to Professor José H. Zagal on the occasion of his 65th birthday, wishing him more and more creative and enjoyable decades.

Armelle Ringuedé and Michel Cassir are members of ISE.

✉ Mosbah Ferkhi
ferkhi_m@univ-jijel.dz

✉ Michel Cassir
michel.cassir@chimie-paristech.fr

[1] Département de Chimie, Faculté des Sciences Exactes et Informatique, Université Mohamed Seddik Ben Yahia—Jijel, BP 98, Ouled Aissa 18000, Jijel, Algérie

[2] PSL Research University, Chimie ParisTech - CNRS, Institut de Recherche de Chimie Paris, 75005 Paris, France

Introduction

Nowadays, it is well known that the best solution to increase the solid oxide fuel cell (SOFC) lifetime is to lower its operating temperature. A good compromise between the durability of materials and the use of coupled thermal and electric energy for cogeneration is to work at intermediate temperatures, <700 °C, in the so-called IT-SOFCs. However, when using the state-of-the-art materials, the decrease in temperature provokes a simultaneous increase in the ohmic drop and electrode overpotentials, which greatly limits cell performance.

Different solutions have been proposed in the literature to solve this problem. One of the solutions consists in decreasing the thickness of the classical electrolyte, yttria-stabilized zirconia (YSZ), in order to maintain a low resistance [1]. We will privilege in this work another route related to the selection of new electrodes, in particular the cathode where the research has been focused on mixed conduction materials (MIEC) for their ability to increase the reaction electrode surface. Lanthanum nickelates ($La_2NiO_{4\pm\delta}$) with a K_2NiF_4 structure, which is a MIEC belonging to the Ruddlesden-Popper ($La_{n+1}Ni_nO_{3n+1}$; $n=1$) (RP) family, have attracted considerable attention as potential cathodes because of their relatively high electronic and ionic conductivities. Their advantage with respect to the classical perovskites is the extension of the electrochemical reaction areas together with the decrease in the ohmic drop [2–4].

A recent study on lanthanum nickelates doped with relatively high amounts of copper in the nickel sites ($La_2Ni_{1-x}Cu_xO_{4+\delta}$) ($x=0.1$–1) [5] has shown that, depending on the copper ratio, the electrical conductivity of the material undergoes a sharp increase because of the presence of copper and a decrease in the activation energy. However, these materials are not chemically stable and, in particular, tend to react with YSZ. Copper promotes the oxidation of Ni^{2+} into Ni^{3+}, which may induce the formation of a layer of lanthanum

Published online: 05 October 2015

zirconate resulting from the diffusion of Cu^{2+} in the electrolyte. This increases the ohmic drop at the electrode/electrolyte interface. Moreover, doping with copper leads to an increase in the grain size and affects the morphology and structure of the material, which has a negative impact on the electrode response [6–8]. $La_2Ni_{1-x}Cu_xO_{4+\delta}$ with x=0.01–0.1 materials have been tested in order to be used as SOFC cathodes [9]. Doping small amounts of copper (x=0.01) in the nickel site provides a pure nickelate material and prevents the formation of undesirable phases. Copper ions improve the electrical properties of the material by creating vacancies so that the electronic conduction increases. However, when the ratio of copper increases, it diffuses in the heart of the electrolyte causing the formation of undesirable phases, which may adversely affect the electrochemical performances. The addition of copper may change the electrode process by decreasing the charge transfer resistance. At small amounts of x=0.01, no secondary phases are detected after heating at 1000 °C for 4 or 48 h. The copper introduced in the nickelate crystalline structure seems to stabilize the material. Recently, the interface between a new composition of non-stoichiometric lanthanum nickelate, $La_{1.98}NiO_{4\pm\delta}$, and YSZ and gadolinia-doped ceria (GDC) has been investigated [10]. XPS analyses have shown that this material has an excess of oxygen with respect to $La_2NiO_{4\pm\delta}$, which favours the ionic transport in the gas/electrode/electrolyte interfaces, resulting in an abrupt decrease in the area specific resistance (ASR) value. Moreover, the use of GDC electrolyte instead of the usual YSZ prevents the formation of undesirable phases at the electrode/electrolyte interface. The electrochemical properties of two cells constituted by GDC or YSZ electrolyte recovered on both faces by the new cathode material have shown that the presence of GDC favours the oxygen reduction at temperatures lower than 680 °C (lower values of ASR and polarization resistance are obtained with respect to YSZ). In this temperature range, charge transfer and ionic transport are enhanced with GDC, probably because of the absence of interfering interfacial phases. At higher temperature, the blocking effect of the electrode and YSZ interface becomes less dramatic.

The n=1 phase, $La_2NiO_{4\pm\delta}$, is known to have a good ionic conductivity but its performance as a single-phase cathode is limited by its electronic conductivity [11–13]. Therefore, this phase has insufficient total conductivity as cathode for IT-SOFC. Thus, two other phases of the RP family with n=2 and 3 were studied. Unlike the first family member (n=1), in these materials the total conductivity is reported to increase with n, corresponding to the thickness of the perovskite slabs in the layered structure [14]. The crystallographic structures of the Ruddlesden-Popper phases (RP) are produced by alternating blocks separated by rock-salt layers, where n corresponds to the number of perovskite blocks, as shown in Fig. 1. Increasing the number of perovskite layers in the Ruddlesden-Popper (RP) nickelates leads to faster ionic and

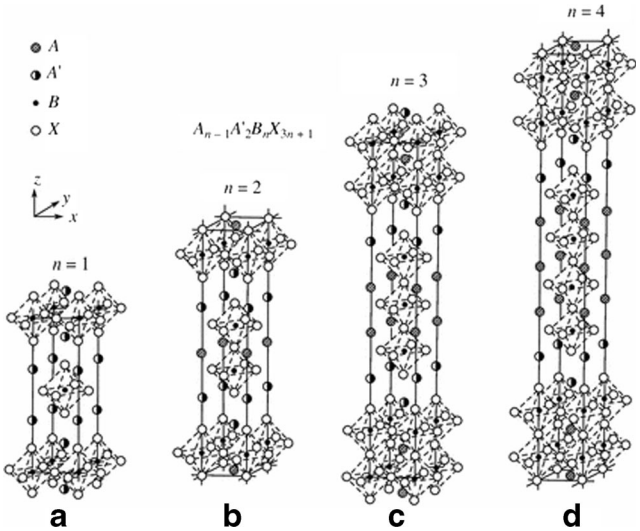

Fig. 1 Crystallographic structures of the Ruddlesden-Popper phases (RP): **a** n=1; **b** n=2; **c** n=3; and **d** n=4

electronic transport [14–17]. These effects are primarily associated with increasing concentration of Ni-O-Ni bonds responsible for the electronic conduction, progressive delocalization of the p-type electronic charge carriers, and increasing vacancy-migration contribution to oxygen ion diffusivity. Note that, except for $La_2NiO_{4\pm\delta}$, all RP nickelates are oxygen-deficient at elevated temperatures [16, 18]. Zhongliang et al. have studied the electrochemical performance of $La_3Ni_2O_7$ with YSZ; its ASR is as low as 0.39 Ω cm^2 at 750 °C [19]. Furthermore, this material presents no visible reaction with YSZ [14]. $La_4Ni_3O_{10}$ materials, studied by Greenblatt et al., are expected to have charge density wave instabilities [20].

Amow et al. have doped cobalt ions in nickel sites in $La_4Ni_{3-x}Co_xO_{10\pm\delta}$ compounds, resulting that all the compositions are oxygen-deficient and two structural types, *Bmab* and *Fmmm*, identified. Increased cobalt substitution results in a systematic decrease in the electrical conductivity from x=0.0 to 2.0, after which a reverse trend is observed with increasing values for x=2.0 to 3.0 [14]. These trends have been interpreted as being associated with the relative changing amounts of the Co^{2+}/Co^{3+} ions as more cobalt is introduced in the solid solution. Finally, when associated in a symmetrical cell with LSGM as electrolyte, the x=0.40 composition shows lower ASR values than the parent nickelate, $La_4Ni_3O_{9.78}$. This, coupled with the relative stability of this phase in air, makes this material a viable candidate for further investigation as IT-SOFC cathodes.

The use of composite materials is to improve performances not evidenced by a single component of the mixture [21]. Recently, Woolley et al. [22, 23] have studied the properties of new composite materials such as cathode for SOFCs consist of $La_2NiO_{4\pm\delta}$ (L2N1) and $La_4Ni_3O_{10-\delta}$ (L4N3). A mixture

of 50:50 wt% between $La_2NiO_{4\pm\delta}$ and $La_4Ni_3O_{10-\delta}$ improved its electrochemical performance with an ASR at 700 °C of 0.62 Ω cm^2 with $La_{0.8}Sr_{0.2}Ga_{0.8}Mg_{0.2}O_{3-\delta}$ (LSGM8282) electrolyte. The formation of a composite leads to improved performance aver the single phases, particularly above 600 °C [22]. The same authors have studied a new architecture, which is composed as follows: − a thin compact L2N1 ($La_2NiO_{4\pm\delta}$) layer adjacent to the electrolyte improving the electrolyte/electrode contact and providing more active sites for oxygen reduction and incorporation; − a thicker more porous L2N1 ($La_2NiO_{4\pm\delta}$)+L4N3 ($La_4Ni_3O_{10-\delta}$) composite, for which a 50:50 wt% mixture gave the best performance [23]. The outer layer of porous L4N3 acts as a low cost current collector. With this configuration, an ASR value as low as 0.53 Ω cm^2 is obtained at 700 °C, which represents the highest performance for these La-NiR-P phases.

Compared to two recent studies dedicated to only one composite material (L2N1+L4N3) [22, 23], the originality of this work is to synthesize and analyse a series of composite materials constituted by $La_2NiO_{4\pm\delta}$, doped in the lanthanum site by copper, and $La_4Ni_3O_{10-\delta}$, with a weight percentage of 50:50 wt%, as cathode materials for SOFC. Doping by copper aims at improving the electrochemical performance of the material and using $La_4Ni_3O_{10-\delta}$ may contribute to stabilize the cathode materials.

Experimental procedure

$La_{2-x}Cu_xNiO_{4+\delta}$ samples with x=0, 0.01, 0.02, 0.05 or 0.1 and $La_4Ni_3O_{10}$ were prepared using the modified Pechini method [24], described and detailed elsewhere [9]. The abbreviation and composition of the different compounds synthesized are summarized in Table 1. La_2O_3, $Ni(NO_3)_2{\cdot}6H_2O$ and $Cu(NO_3)_2{\cdot}3H_2O$ reagents were used as starting materials, with a purity of 99.99, >98 and 99 %, respectively. Lanthanum oxide was first dissolved in dilute nitric acid. Nickel and copper nitrates in appropriate quantities were dissolved in water and added to the lanthanum solution. An excess of ethylene glycol (EG) and citric acid (CA) mixture was then added drop wise as curing agents. The solution was stirred at 75 °C until a viscous mixture was obtained. The product was then dried at 120 °C. The powder was crushed in a mortar and sintered under different temperatures, from 200 to 500 °C, for 1 h to remove organic materials. The final product was annealed at 1000 °C for 5 h in air. A 50:50 wt% $La_{2-x}Cu_xNiO_{4+\delta}$ (x=0.01–0.1) and $La_4Ni_3O_{10}$ mixtures were examined. The phase nature and purity for each mixture was confirmed by X-ray diffraction (XRD). The ink composed by $La_{2-x}Cu_xNiO_{4+\delta}$ (x=0.01–0.1), $La_4Ni_3O_{10}$ and glycol ethylene (GE) (one drop GE for 100 mg powder) was then painted on both sides of YSZ (with 8 mol% of Y_2O_3) pellet used as electrolyte (obtained by pressing under 1508.15 MPa for 5 min, then sintered at 1400 °C for 1 h). The density of the pellet is about 94 % with a thickness of 1 mm and a diameter of 0.8 cm.

XRD with a Philips PW 1390 diffractometer using the Co Kα radiation (1.78897 Å), with 2θ varying from 20° to 80°, was used to characterize the synthesized samples and analyse the phase composition. The diffraction pattern was scanned by steps of 0.02° with 2 s counting times. Scanning electron microscopy, SEM (S440, FEG from LEICA), coupled with energy dispersive X-ray spectrometry, EDS (S440, FEG from LEICA) was used to investigate the morphology of the different samples. Electrochemical measurements were performed using a PGSTAT 20 Potentiostat, AutoLab Ecochem BV (Amsterdam, The Netherlands) in a temperature range between 400 and 800 °C in air, under a pressure of 1 atm, in the 1 MHz–10^{-2} Hz frequency range (11 points per decade of frequencies) with a signal amplitude of 50 mV (in respect to the system linearity). The symmetrical cells $La_{2-x}Cu_xNiO_{4\pm\delta}$+$La_4NiO_{10}$/YSZ/$La_{2-x}Cu_xNiO_{4\pm\delta}$+$La_4NiO_{10}$ with x=0.01, 0.02, 0.05 and 0.1 were annealed, respectively, at 350 °C for 1 h and then sintered at 900 °C for 5 h, so that a good adhesion between the electrolyte and the deposited layers was obtained. Spiral Pt wires (0.8 cm diameter) were placed on both sides of the cell as current collectors. The names of the different cells studied are as follows: cell 1, L1NC+L4NO/YSZ/L1NC+L4NO; cell 2, L2NC+L4NO/YSZ/L2NC+L4NO; cell 3, L5NC+L4NO/YSZ/L5NC+L4NO and cell 4, L10NC+L4NO/YSZ/L10NC+L4NO.

Table 1 Abbreviation and composition of pure phases

Composition	Abbreviation
$La_{1.99}Cu_{0.01}NiO_{4\pm\delta}$	L1NC
$La_{1.98}Cu_{0.02}NiO_{4\pm\delta}$	L2NC
$La_{1.95}Cu_{0.05}NiO_{4\pm\delta}$	L5NC
$La_{1.90}Cu_{0.10}NiO_{4\pm\delta}$	L10NC
$La_4Ni_3O_{10-\delta}$	L4NO

Results and discussion

XRD analysis

XRD analyses of $La_{2-x}NiCu_xO_{4\pm\delta}$ (x=0, 0.01, 0.02, 0.05 and 0.1) and L4NO are shown in Fig. 2. The doping of lanthanum sites by copper leads to the formation of pure phases with a K_2NiF_4 structure, in agreement with several studies [8–10, 25–28]. It is likely that cupric ions replace lanthanum sites and create additional sites displacement, which improves the electrical conductivity. Figure 2(e) depicting the XRD patterns of ($La_{n+1}Ni_nO_{3n+1}$; n=3), noted L4NO ($La_4Ni_3O_{10}$), confirms the formation of RP

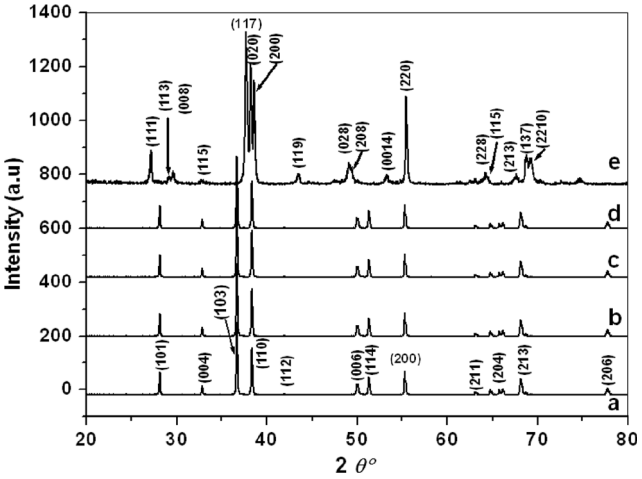

Fig. 2 XRD of the following cathode materials: (*a*) L1NC; (*b*) L2NC; (*c*) L5NC; (*d*) L10NC; (*e*) L4NO, as-prepared after annealing for 1000 °C in air

phases, which is in accordance with the literature [22, 23]. The pellets resulting from the mixture of $La_{2-x}NiCu_xO_{4\pm\delta}$ (x=0, 0.01, 0.02, 0.05 and 0.1) and $La_4Ni_3O_{10-\delta}$ (L4NO) materials, annealed at 900 °C for 5 h, deposited on YSZ electrolyte, was analysed by XRD, as shown in Fig. 3, with the identification of the peaks corresponding to the

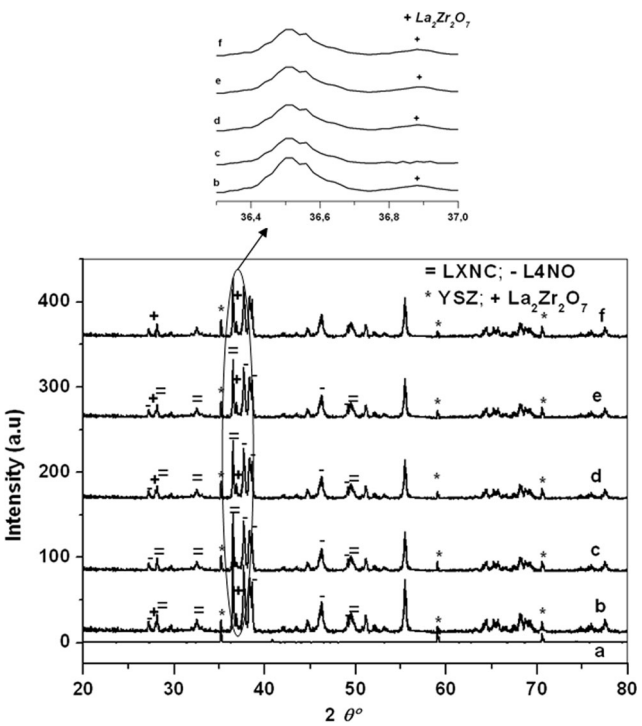

Fig. 3 XRD of the following materials and half-cells (after heating for 900 °C in air for 5 hours), including details on insulating phases (after scratching part of the cathode layer): (*a*) YSZ support; (*b*) YSZ/L1NC+L4NO; (*c*) YSZ/L2NC+L4NO; (*d*) YSZ/L5NC+L4NO; (*e*) YSZ/L10NC+L4NO

different structural phases. After scratching part of the cathode layer, the presence of a secondary phase at the interface with the electrolyte can be noted for the following samples: L1NC+L4NO/YSZ, L5NC+L4NO/YSZ and L10NC+L4NO/YSZ. The small peaks identified for this phase are characteristic of lanthanum zirconate ($La_2Zr_2O_7$), a blocking phase due to the reaction of cathode material with the electrolyte material; however, this phase seems totally absent at the interface between L2NC+L4NO and the electrolyte, which is difficult to fully understand at this stage of the study, probably due to a combination of low doping amounts of copper and the presence of $La_4Ni_3O_{10}$ acting as a stabilizer of the material at high temperature.

Morphological analysis

Figure 4 shows SEM micrographs of the heat-treated powders constituted by a mixture by $La_{2-x}NiCu_xO_{4\pm\delta}$ ($0.01 \leq x \leq 0.1$) and L4NO. In the case of the samples doped with copper, the general tendency when increasing the amount of copper is that the grains become more coalesced and the samples less porous. For higher doping amounts of copper with $x \geq 0.05$, the samples are more coalesced and less porous than $La_4Ni_3O_{10}$ sample. According to the literature [29], $La_2NiO_{4\pm\delta}$ powder heated at 1000 °C for 2 h crystallizes in the orthorhombic system (spatial group F_{mmm}) with spherical elementary particles of 150 nm. However, for $La_4Ni_3O_{10}$ (L4NO), the grains are larger, less porous and they have an acicular geometry. Heat treatment of the compound at 1000 °C for 2 h increases the diameter of the particles (200×600 nm). These results are in agreement with the literature [9, 10]. The presence of L4NO tends to change the geometry of particles, increasing their size and their coalescence, as can be seen in Fig. 5. The porosity of the samples is also reduced with the addition of L4NO; however, there is significant difference between the samples. L2NC+L4NO and L5NC+L4NO are significantly more porous than the two other samples L1NC+L4NO and L10NC+L4NO, showing that doping with 2 and 5 % of copper is more favourable than with 1 or 10 %. It is difficult at this stage to have a precise explanation on these behaviours, but one may conclude that doping with copper and addition of L4NO affect significantly the morphology and porosity of the samples and, therefore, might affect negatively or positively the electrochemical performance of the materials. The sample doped with 2 %, more porous and not presenting an insulating phase appears to be of particular interest but only a thorough electrochemical analysis can allow us to conclude.

Figure 6 depicts the SEM micrograph cross-sections of the pellets constituted by LXNC+L4NO samples

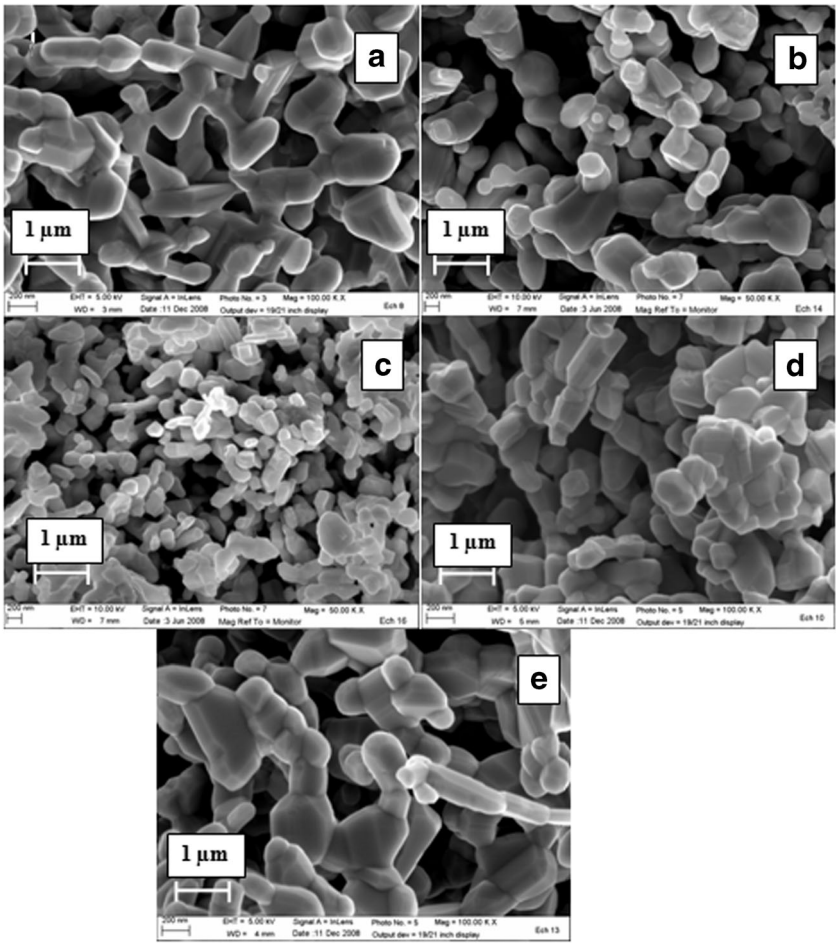

Fig. 4 SEM micrographs of the single samples heat-treated and before mixing: **a** L1NC; **b** L2NC; **c** L5NC; **d** L10NC; and **e** L4NO

deposited on YSZ. The thickness of all the samples is around 40 µm, as shown in Fig. 6a in the case of L1NC+L4NO. The quality of the interfaces between the cathode and the YSZ electrolyte can be clearly observed. It can be concluded that there is a good adhesion between the deposited porous layers and the dense electrolyte.

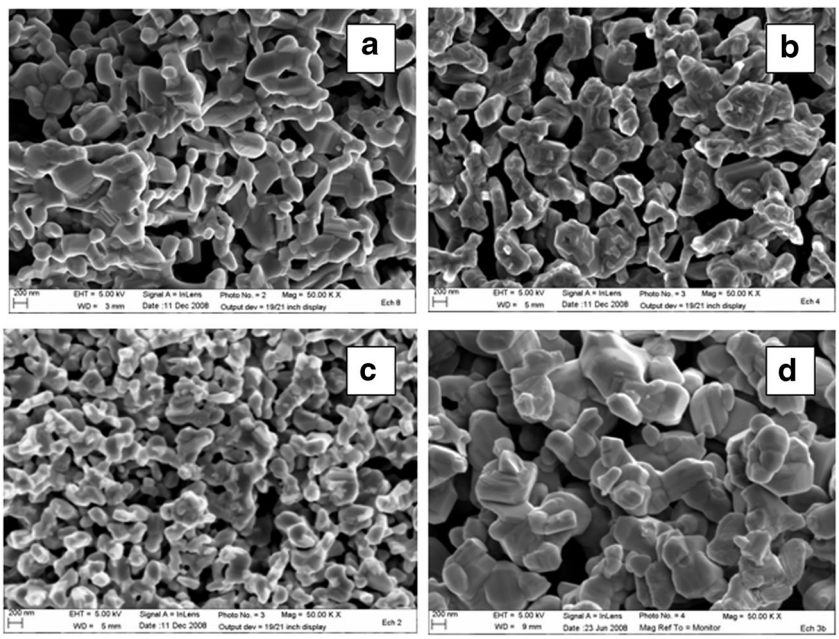

Fig. 5 SEM micrographs of $La_{2-x}NiCu_xO_{4\pm\delta}$+L4NO samples for: **a** L1NC+L4NO; **b** L2NC+L4NO; **c** L5NC+L4NO; **d** L10NC+L4NO

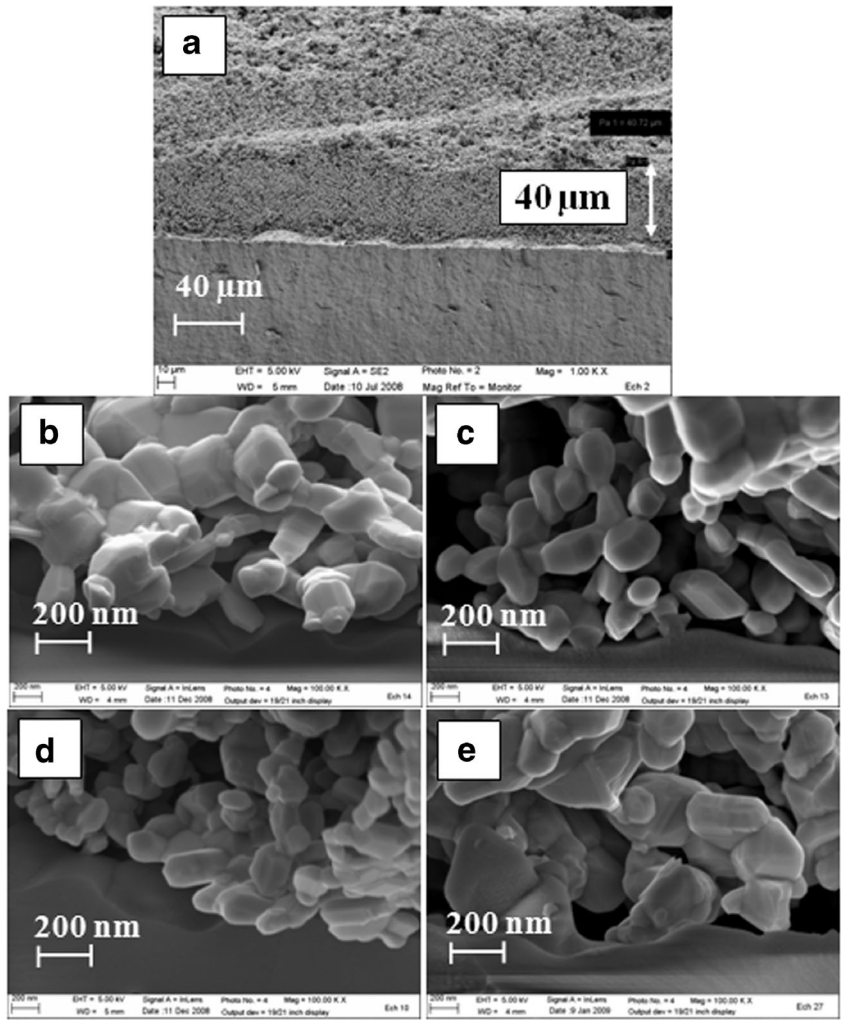

Fig. 6 SEM micrographs showing cross-sections of LXNC+L4NO layers deposited on YSZ substrate: **a** thickness of L1NC+L4NO; **b** L1NC+L4NO with magnification; **c** L2NC+L4NO; **d** L5NC+L4NO; and **e** L10NC+L4NO

Electrochemical performances

Typical impedance spectra (Nyquist representation) were obtained in a temperature range of 550–800 °C for all the symmetrical cells: cell1, cell2, cell3 and cell4. The example of cell2 is given at 550 °C in Fig. 7, showing experimental and deconvoluted Nyquist plots. Each contribution, represented by a semi-circle in the decomposition of the impedance diagrams, was simulated by an electrical equivalent circuit corresponding to a parallel association of a resistance and a constant phase element, RQ. The entire equivalent circuit is the association in series of all RQ. In the case of this cell, one semi-circle is observed at high frequency, HF (between 1 MHz and 100 kHz), which is not influenced by signal amplitude variation (from 20 to 300 mV, results not shown here) and can be ascribed to the electrolyte contribution. Two main semi-circles are observed, respectively, at medium frequency (MF), located between 1000 and 1 Hz, and at low frequency (LF), between 1 Hz and 10 mHz [30]. They can be attributed to charge transfer at the electrode/electrolyte interface and transport phenomena, respectively. The same general shapes are obtained for the others cells.

Figure 8 compares the impedance spectra at 550 °C obtained with the four configurations: L1NC+L4NO, L2NC+L4NO, L5NC+L4NO and L10NC+L4NO, and shows drastic changes for the different samples. At the selected temperature, the total resistance of the L5NC+L4NO/YSZ system, very close to that of L2NC+L4NO/YSZ, is significantly lower than the two other cells. At 550 °C, the resistance of the YSZ electrolyte is not the same for all the samples considered. Higher values are obtained with the L1NC+L4NO, L5NC+L4NO and L10NC+L4NO electrodes, which could originate from the formation of the secondary lanthanum zirconate phase previously detected. Concerning the electrode contribution, as a first approach, we have simulated each arc through an equivalent circuit constituted by a resistance in parallel with a constant phase element (CPE), in order to follow the variations of the equivalent capacitances and the corresponding resistances. Furthermore, impedance spectra show that the resistances corresponding to medium

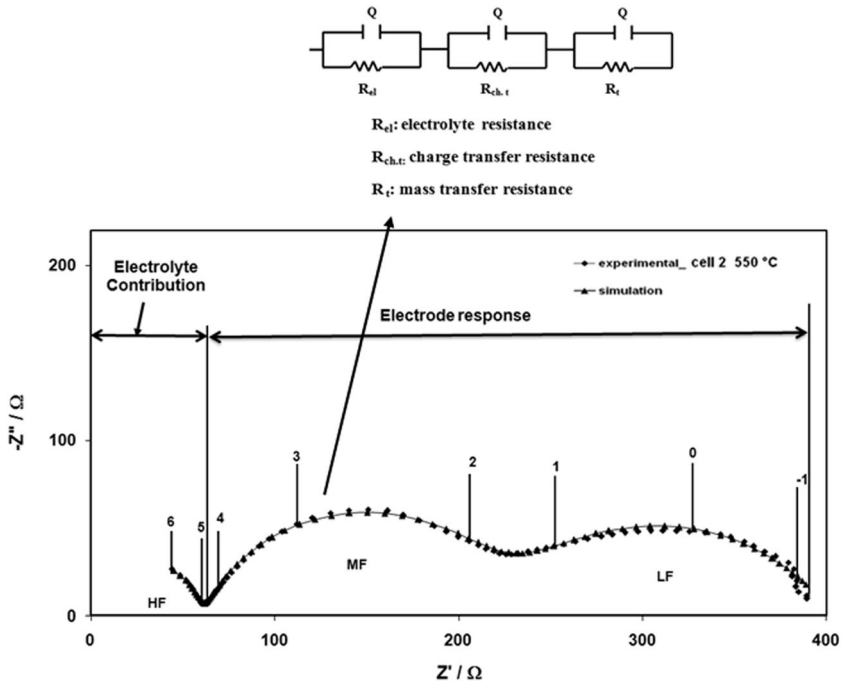

Fig. 7 Experimental, simulated Nyquist impedance diagrams and equivalent circuit obtained at 550 °C with an amplitude of 50 mV for cell2

frequencies are always the largest, which indicate that the limiting step of the overall reaction of oxygen reduction is charge transfer at the electrode/electrolyte interface. As can be deduced from Fig. 9a, b, capacity (C_m) average values, deduced from semi-circles at low and medium frequencies, are respectively around 10^{-4} and 10^{-7} F cm^{-2}, which corresponds to the phenomena associated to the electrode reactions (sorption phenomena of oxygen species, dissociation-

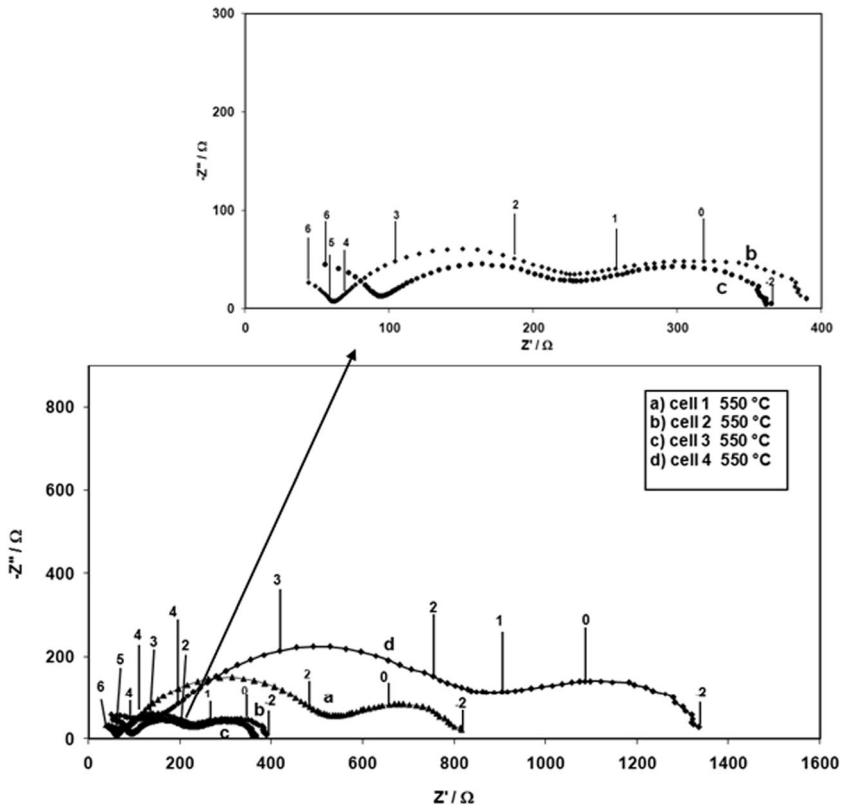

Fig. 8 Typical Nyquist diagrams at 550 °C for all the cells

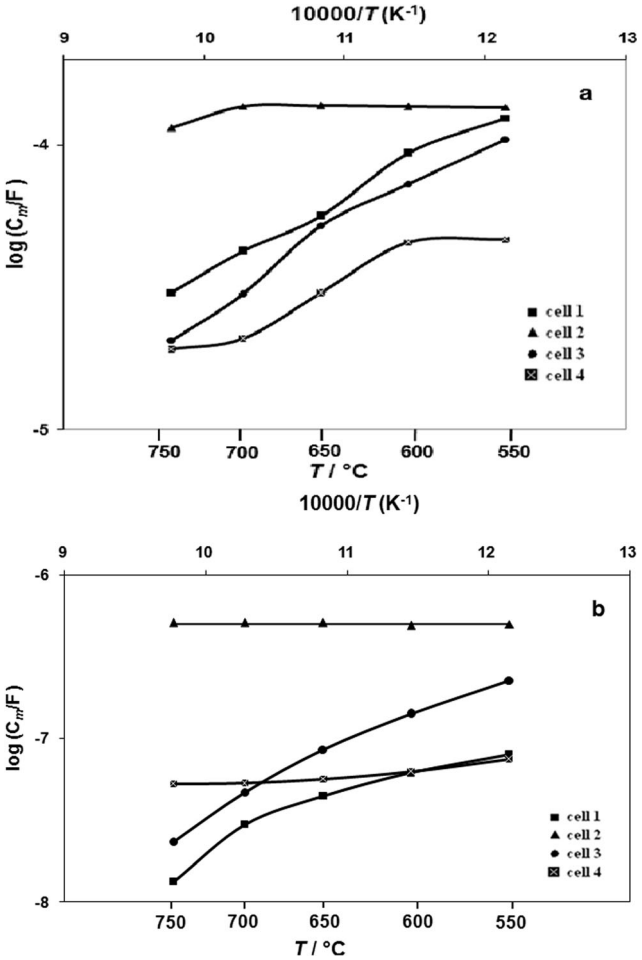

Fig. 9 Average capacity, C_m, for $La_{2-x}NiCu_xO_{4\pm\delta}$ system characteristic of **a** low frequency and **b** medium frequency semicircles

reduction of oxygen, diffusion within the cathode material…) and the cathode/electrolyte interface, respectively [30]. It is interesting to outline that for cell2, both capacities

Table 2 Activation energy of LXNC and L4NO mixtures

Sample	Activation energy (eV)
L1NC+L4NO	1.16±0.05
L2NC+L4NO	1.20±0.05
L5NC+L4NO	1.02±0.05
L10NC+L4NO	1.20±0.05

are at medium and low frequencies and independent on time, which show the stability of this sample, which is the only one not presenting and insulating phase at the interface cathode/electrolyte. Figure 10 represents the Arrhenius plots normalized using log ASR for $La_{2-x}NiCu_xO_{4\pm\delta}$ ($0.01 \leq x \leq 0.1$)+L4NO as-prepared materials. The values of the activation energies given in Table 2 are similar (around 1.2±0.05 eV), except for L5NC+L4NO and L1NC+L4NO samples with a lower value of 1.0±0.05 eV. It can be noted that for this last sample, oxygen reduction process seems to be favoured in spite of the insulating phase detected, which can also be due to the positive influence of L4NO material on the electrochemical properties of the mixture. Another important observation is that ASR values are significantly lower for L5NC and L2NC-based compounds, three to five times less than for the two other samples, deducing that doping with 2 or 5 % of copper is the most favourable ratio.

Comparative data between these two last half-cells (with $x=0.02$ and 0.05) and the reference cell constituted by undoped $La_2NiO_{4\pm\delta}$ deposited on YSZ electrolyte is depicted in Fig. 11. ASR values are significantly lower for the two composites with respect to $La_2NiO_{4\pm\delta}$, clearly showing that the presence of copper improves the electrical properties of the material by creating vacancies favouring electronic conduction. At temperatures below 650 °C, ASR

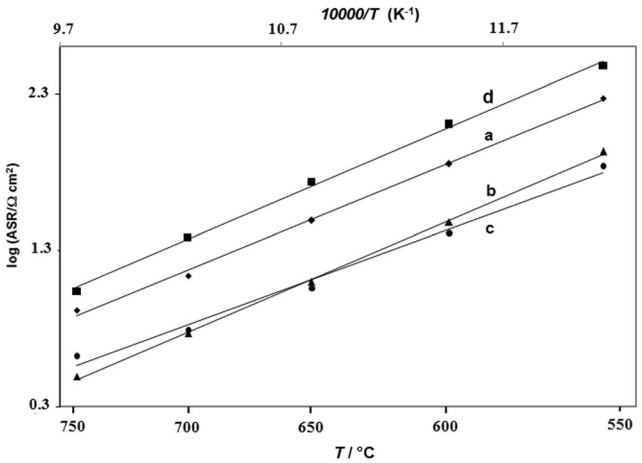

Fig. 10 Arrhenius plots normalized with Log ASR for: (*a*) L1NC+L4NO, (*b*) L2NC+L4NO, (*c*) L5NC+L4NO and (*d*) L10NC+L4NO half-cells

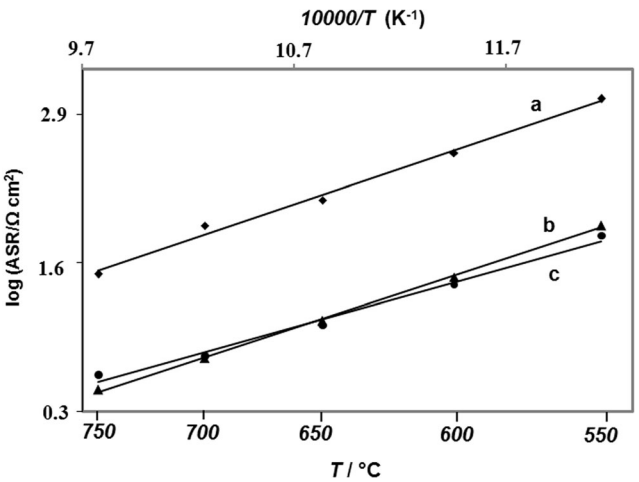

Fig. 11 Comparative ASR data for: (*a*) non-doped $La_2NiO_{4\pm\delta}$ [9, 10], (*b*) L2NC+L4NO and (*c*) L5NC+L4NO materials on YSZ electrolyte

Table 3 ASR values compared with other works

Electrode/electrolyte	*T*, °C	ASR values (Ω cm^2)	Ref
$La_2Ni_{1-x}Cu_xO_4$/LSGM (x=0.4 and 0.6)	850	1	[5]
$La_2Ni_{1-x}Cu_xO_{4\pm\delta}$/YSZ	650	100	[9]
	750	17	
$La_{1,98}NiO_{4\pm\delta}$/YSZ	650	63	[10]
	750	10	
$La_{1,98}NiO_{4\pm\delta}$/YSZ	750	9	[27]
$La_2NiO_{4\pm\delta}$/YSZ	650	30.7	[30]
	750	7.8	
$La_4Ni_{3-x}Co_xO_{10\pm\delta}$/LSGM	650	17.7	[31]
	750	3.1	
$La_2NiO_{4\pm\delta}$/CGO	650	10	[32]
	750	5.6	
$La_{1.98}Cu_{0.02}NiO_{4\pm\delta}$+$La_4Ni_3O_{10}$	650	11.8	This work
	750	2.8	
$La_{1.95}Cu_{0.05}NiO_{4\pm\delta}$+$La_4Ni_3O_{10}$	650	11,8	This work
	750	3.5	

values of the L5NC+L4NO cathode are slightly lower than those of L2NC+L4NO (24 and 26 Ω cm^2 at 600 °C, respectively). A possible explanation is that oxygen reduction is facilitated in the case of L5NC+L4NO because of its higher porosity. At temperature above 650 °C, the tendency is reversed, which could probably be due to the influence of the secondary phase formed in the case of the L5NC+L4NO cathode. Finally, L2NC+L4NO cathode with an acceptable electrochemical behaviour and the absence of any insulating phase seems to be the best choice and in particular at $T\geq$ 650 °C. It is interesting to note that the values of ASR are significantly lower than those obtained in previous works on $La_{1.98}NiO_{4\pm\delta}$ (10 Ωcm^2 at 750 °C [10]) or $La_2Ni_{0.99}Cu_{0.01}O_{4\pm\delta}$ (23 Ωcm^2 at 750 °C [9]).

Table 3 contains the different values of ASR obtained in this work and in the literature. Even though, we are conscious that the microstructure of our samples should be improved, allowing to obtain better performance, we already succeeded in obtaining promising electrochemical properties in comparison with the literature.

Conclusion

Composite materials constituted by nickelates, $La_{2-x}NiCu_xO_{4\pm\delta}$ (x=0.01, 0.02, 0.05 and 0.1) and $La_4Ni_3O_{10}$, were successfully prepared by the Pechini method using ethylene glycol and citric acid as complexing agent. Doping with x=0.02 produced a pure nickelate material without any additional phase in contact with YSZ electrolyte. Other amounts of copper conduced to an undesirable lanthanum zirconate phase at the interface with the electrolyte, affecting the electrochemical performance of the corresponding symmetrical cells. The best electrochemical performance was obtained with the composites half-cells: L5NC+L4NO and L2NC+L4NO, knowing that the 5 % Cu sample has the lowest ASR at T>650 °C and the 2 % Cu sample the lowest ASR at T<650 °C. Both samples show a better electrochemical behaviour that undoped $La_2NiO_{4\pm\delta}$. The positive role of L4NO phase in the composite was outlined, in particular in the case of L5NC+L4NO at T>650 °C. Furthermore, the average capacity at medium and low frequency of the L2NC+L4NO cell is stable with respect to temperature, contrarily to the other configurations. We can conclude that the L2NC+L4NO composite material, without any undesirable phase at the interface with the electrolyte, appears as the most interesting one for SOFC applications, combining the benefit of the 2 % Cu-doped nickel lanthanate and the L4NO material.

References

1. Steele BCH, Heinzel A (2001) Materials for fuel-cell technologies. Nature 414:345–52
2. Bouwmeester HJM, Burgraaf AJ (1996) In: Burgraaf AJ, Cot L (eds) Fundamentals of inorganic membrane science and technology. Amsterdam, Elsevier
3. Kharton VV, Viskup AP, Kovalevsky AV, Naumovich EN, Marques FMB (2001) Solid State Ionics 143:337–353
4. Soorie M, Skinner SJ (2006) Solid State Ionics 177:2081–2086
5. Aguadero A, Alonso JA, Escudero MJ, Daza L (2008) Solid State Ionics 179:393–400
6. Kharton VV, Yaremchenko AA, Tsipis EV, Valente AA, Patrakeev MV, Shaula A (2004) Appl Catal A Gen 261:25–35
7. Tsipis EV, Naumovich EN, Patrakeev MV, Waerenborgh JC, Paivak YV, Gaczynski P, Kharton VV (2007) J Phys Chem Solids 68:1443–1455
8. Zhao H, Mauvy F, Lalanne C, Bassat JM, Fourcade S, Grenier JC (2008) Solid State Ionics 179:2000–2005
9. Ferkhi M, Khelili S, Zerroual L, Ringuedé A, Cassir M (2009) Electrochim Acta 54:6341–6346
10. Ferkhi M, Ringuedé A, Khaled A, Zerroual L, Cassir M (2012) Electrochim Acta 75:80–87
11. Minervini L, Grimes RW, Kilner JA, Sickafus KE (2000) J Mater Chem 10:2349–2354
12. Bassat JM, Odier P, Villesuzanne A, Marin C, Pouchard M (2004) Solid State Ionics 167:341–347
13. Chroneos A, Parfitt D, Kilner JA, Grimes RW (2010) J Mater Chem 20:266–272
14. Amow G, Davidson IJ, Skinner SJ (2006) Solid State Ionics 177: 1205–1210
15. Al Daroukh M, Vashook VV, Ullmann H, Tietz F, Raj IA (2003) Solid State Ionics 158:141–150
16. Zhang Z, Greenblatt M (1995) J Solid State Chem 117:236–246
17. Kharton VV, Yaremchenko AA, Naumovich EN (1999) J Solid State Electrochem 3:303–326
18. Bannikov DO, Cherepanov VA (2006) J Solid State Chem 179: 2721–2727
19. Lou Z, Peng J, Dai N, Qiao J, Yan Y, Wang Z, Wang J, Sun K (2012) Electrochem Commun 22:97–100
20. Greenblatt M, Zhang Z, Whangbo MH (1997) Synth Met 85: 1451–1452

21. Rieu M, Sayers R, Laguna-Bercero MA, Skinner SJ, Lenormand P (2010) J Electrochem Soc 157:B477–484
22. Woolley RJ, Skinner SJ (2013) J Power Sources 243:790–795
23. Woolley RJ, Skinner SJ (2014) Solid State Ionics 255:1–5
24. Pechini (1967) US Patent 3;330–697
25. Montenegro Hernandez A, Mogni L, Caneiro A (2010) Int J Hydrog Energy 35:6031–6036
26. Solís C, Navarrete L, Serra JM (2013) J Power Sources 240:691–697
27. Lenormand P, Rieu M, Cienfuegos RF, Julbe A, Castillo S, Ansart F (2008) Surf Coat Technol 203:901–904
28. Li Z, Haugsrud R, Smith JB, Norby T (2009) Solid State Ionics 180:1433–1441
29. Jorgensen JD, Dabrowski D, Pei S, Richards DR, Hinks DG (1989) Phys Rev B 40:2187–2194
30. Escudero MJ, Aguader A, Alonso A (2007) J Electroanal Chem 611:107–116
31. Amow G, Au J, Davidson I (2006) Solid State Ionics 177:1837–1841
32. Sayers, Rieu M, Lenormand P, Ansart F, Kilner JA, Skinner SJ (2011) Solid State Ionics 192:531–534